WEP Warwick Evans Publishing

International Journal of Natural Resources and Environmental Studies

ISSN: 3006-2012 (Print), ISSN: 3006-0834 (Online) | Volume 8, Number 3, Year 2026
DOI: https://doi.org/10.62051/ijnres.v8n3.19
Journal homepage: https://wepub.org/index.php/IJNRES/index

Petrogenesis of the Heyu Megaporphyritic Coarse-grained Monzogranite in the Baimiaogou Area, Western Henan: Petrological Evidence

Xinhang Zhou*

Institute of Resources & Environment, Henan Polytechnic University, Jiaozuo 454000, China
*Corresponding Author: Xinhang Zhou

ABSTRACT

The Heyu megaporphyritic coarse-grained monzogranite, located in the East Qinling area at the southern margin of the North China Craton, shows a distinctive sub-porphyritic texture and complex mineral assemblages that record the processes of magma formation and emplacement. Field investigations, petrography, and in-situ laser Raman spectroscopy reveal the micro-crystallization characteristics and fluid metasomatic sequences of the primary mineral phases. Early-crystallized plagioclase forms a rigid crystal framework (65% to 70% by volume) that records multiple stages of patchy albitization, K-feldspathization, and silicification. Mafic minerals (hornblende and biotite) and accessory phases (apatite, sphene, zircon, and magnetite) fill intergranular fractures within the felsic framework. These textures suggest precipitation from late-stage volatile-rich hydrothermal fluids rather than normal fractional crystallization. Petrographic evidence defines three dynamic stages of pluton evolution: early crystallization and cold storage of the crystal mush, deep fluid injection and mush reactivation, and magma emplacement with late-stage fluid precipitation. The large-scale influx of deep alkali-rich and volatile-rich supercritical fluids causes intense fluid-rock interaction, significantly reducing the rheological viscosity of the crystal mush. This viscosity reduction is the key mechanism to overcome the rheological barrier of high-silica magmas and facilitate final emplacement.

KEYWORDS

Heyu granite; Crystal mush activation; Fluid metasomatism; East Qinling.

1. INTRODUCTION

The East Qinling area at the southern margin of the North China Craton is a Mesozoic molybdenum polymetallic metallogenic belt, where widely exposed Yanshanian granitic batholiths are spatially and genetically associated with regional mineralization[1-8]. The Heyu megaporphyritic coarse-grained monzogranite in the Baimiaogou area is a typical intrusion within this belt. Its distinctive texture and complex mineral assemblages provide a detailed record of magmatic evolution and late-stage fluid activity. Large felsic magmatic systems are currently understood to reside in the deep crust as high-crystallinity mushes that mobilize and emplace upon fluid reactivation. While zircon geochronology and isotope geochemistry establish a broad spatio-temporal framework for regional magmatism and mineralization, the microscopic mechanisms enabling high-silica, high-viscosity frozen magma chambers to overcome rheological barriers remain poorly constrained[9,10]. Traditional whole-rock geochemistry cannot fully resolve the fine-scale fluid activity and crystal growth dynamics characteristic of terminal magmatic stages. The sub-porphyritic texture of the Heyu

monzogranite provides a direct petrological record of long-term crystal mush cold storage and subsequent multi-stage metasomatism.

This study combines detailed field mapping, petrography, and in-situ laser Raman spectroscopy to determine the micro-crystallographic characteristics and metasomatic sequences of key mineral phases in the Yanshanian Heyu monzogranite. Documenting the multi-stage fluid metasomatism and micro-fracture filling processes provides strict micro-mineralogical constraints on the reactivation and emplacement history of high-silica crystal mushes in the East Qinling belt.

2. REGIONAL GEOLOGY

The study area is located at the southern margin of the North China Craton, featuring a crystalline basement and an overlying sedimentary cover. Three main geological units are exposed in the region. Archean to Paleoproterozoic medium- to high-grade metamorphic rocks form the Precambrian crystalline basement. Mesoproterozoic to Paleozoic volcanic, clastic, and carbonate rocks overlie this basement and show varying degrees of deformation and metamorphism. Jinningian, Caledonian, and Yanshanian intrusive rocks, predominantly granites, intrude the sequence. The large-scale emplacement of Yanshanian granitic magma is controlled by regional tectonic regime transitions and deep magmatic activity [11-14].

The area is extensively faulted, with intersecting west-northwest, east-northeast, near-east-west, and near-north-south structures modifying one another [15,16]. The intersection of the northwest-trending Dianfang-Puchi fault zone and the northeast-trending Heyu-Muzhijie fault zone forms a semi-annular structure protruding to the northwest. The megaporphyritic coarse-grained monzogranite is emplaced at this structural apex, intruding altered andesites of the Xiong'er Group to the southeast.

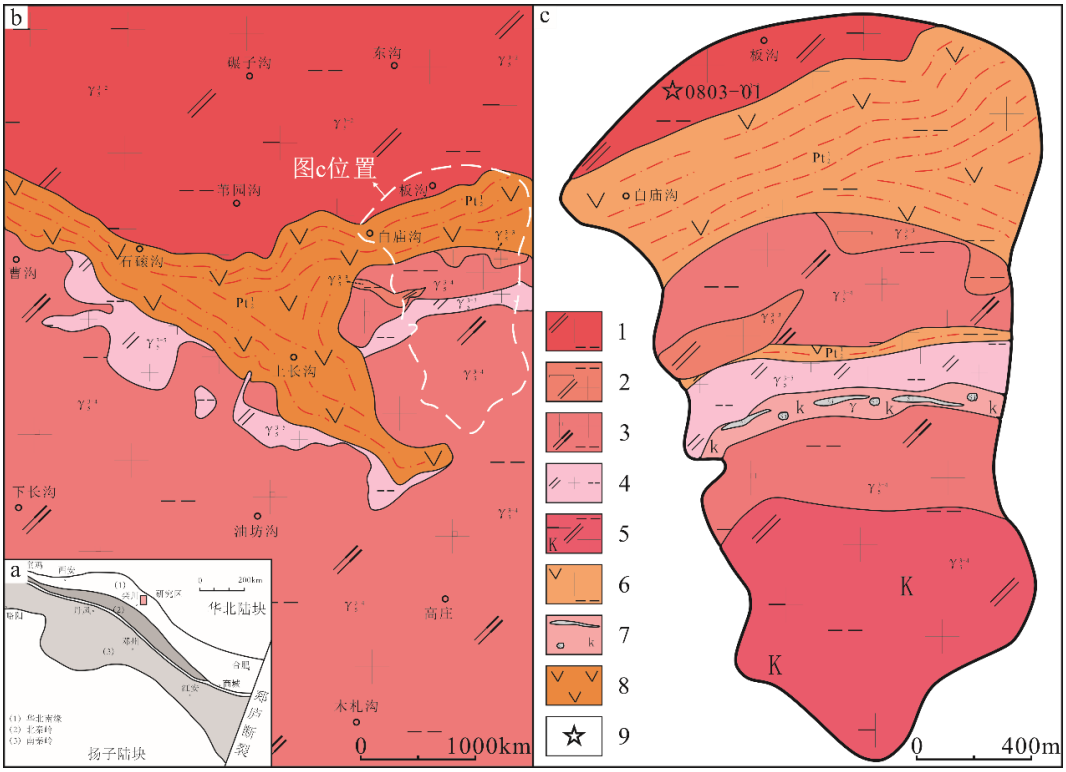

Fig. 1 Tectonic location and simplified geological map of the Baimiaogou area in western Henan at the southern margin of the North China Craton. (a) Tectonic location of the study area; (b) Simplified geological map of the study area; (c) Geological map of the Heyu granite in Baimiaogou. 1 Megaporphyritic coarse-grained granite; 2 Medium-coarse-grained granite; 3 Medium-grained granite; 4 Fine-grained granite; 5 K-feldspathized medium-grained granite; 6 Meta-andesite; 7 K-feldspathized zone locally intercalated with silicified nodules; 8 Andesite; 9 Sampling location.

3. SAMPLE COLLECTION AND ANALYTICAL METHODS

3.1. Sample Collection

Samples of the megaporphyritic coarse-grained monzogranite (Sample No. 0803-01) are collected from the northwestern sector of the Baimiaogou molybdenum deposit. The rock is massive and sub-porphyritic, containing flesh-red K-feldspar phenocrysts (1 to 3 cm; 10% to 25% by volume) within a greyish-white groundmass. The groundmass consists of plagioclase (30% to 40%) and smoky-grey quartz (9% to 15%), with grain sizes between 0.1 and 0.5 cm.

3.2. Analytical Methods

Standard 2.5 by 5 cm polished thin sections are prepared for microstructural and petrogenetic analysis. High-resolution images are generated via automatic scanning and photo stitching under plane-polarized, cross-polarized, and reflected light using an Axio Imager M2 research-grade microscope. The microscope is equipped with an ICCS optical system and a motorized scanning stage.

In-situ laser Raman spectroscopy is conducted at the Analytical and Testing Center of Henan Polytechnic University using a WITec alpha300R high-resolution confocal imaging spectrometer. Analytical conditions include a 532 nm laser wavelength, a minimum spot size of 1 μm, and a spectral resolution of less than 1.5 cm^{-1} over a range of 10 to 3900 cm^{-1}.

4. ANALYTICAL RESULTS

4.1. Optical Mineralogy

The monzogranite is porphyritic, consisting of phenocrysts and a groundmass. K-feldspar forms the primary phenocryst phase, while the groundmass consists of plagioclase, quartz, and mafic minerals. K-feldspar grains (4 to 50 mm) are anhedral and interstitial to plagioclase and quartz. Grain margins are often embayed and show perthitic textures, consisting of a K-feldspar host (first-order grey) and exsolved albite lamellae (first-order yellow) with approximately 17% modal abundance. The perthite contains inclusions of vermicular quartz and fragmented plagioclase, the latter occasionally developing clean rims. Mafic minerals frequently concentrate along the perthite boundaries. Plagioclase (approximately 61% modal abundance) occurs as tabular euhedral crystals that commonly show polysynthetic twinning and marginal dissolution textures. Grain cores are frequently altered to argillaceous patches and fine scaly sericite. Anhedral patches with lower refractive indices and high interference colors occur along plagioclase rims. Quartz (13% modal abundance; 0.5 to 20 mm) is anhedral and rough-surfaced, containing inclusions of kaolinized material, plagioclase, and mafic phases. Rare quartz grains pseudomorph earlier plagioclase.

Mafic minerals, predominantly hornblende and biotite, concentrate along the boundaries of felsic phases, forming discontinuous bands 1 to 5 mm wide. Hornblende (5% modal abundance; 0.1 to 1.5 mm) forms rhombic to long-columnar crystals that display two sets of cleavage and light green to brownish-tan pleochroism. Most hornblende grains are partially replaced by biotite and chlorite. Biotite (6% modal abundance; 0.5 to 1.0 mm) occurs as tabular euhedral grains or anhedral patches, the latter commonly replacing hornblende.

Accessory phases include apatite, sphene, zircon, rutile, and magnetite. These minerals are closely associated with mafic phases, occurring as inclusions or along grain margins within the narrow intergranular bands. Apatite forms hexagonal euhedral crystals, while sphene occurs as rhombic euhedral grains. Zircon, characterized by pleochroic halos and extremely high positive relief, forms inclusions within hornblende and biotite, occasionally aligning with biotite cleavage planes. Acicular rutile also tracks along biotite cleavage. Magnetite occurs as subhedral to euhedral polygonal grains

along mafic mineral margins, frequently showing rough crystal faces and etch pits under reflected light.

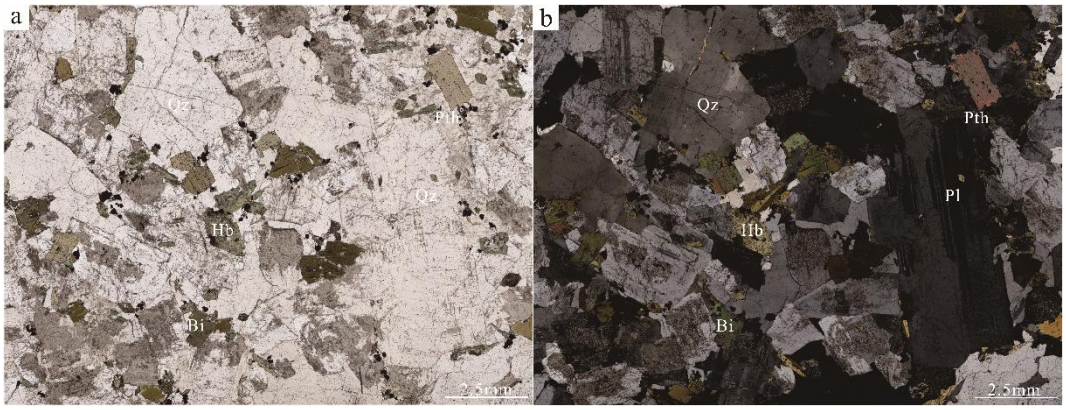

Fig. 2 Optical mineralogical characteristics of the Heyu megaporphyritic coarse-grained monzogranite in the Baimiaogou molybdenum deposit. (a) Plane-polarized light image of the megaporphyritic coarse-grained monzogranite (Sample No. 0803-01); (b) Cross-polarized light image of the megaporphyritic coarse-grained monzogranite (Sample No. 0803-01).

4.2. Laser Raman

Laser Raman spectroscopy is used to confirm the identities of primary, mafic, and accessory phases. The marginal patches on plagioclase grains with low refractive indices are confirmed to be albite. Feldspar rims surrounding the internal argillized and sericitized zones show the Raman spectral peaks of orthoclase. Inclusions within biotite show the characteristic peaks of apatite and rutile. Marginal dissolution is evident on the apatite grains, which Raman frequency shifts identify as fluorapatite.

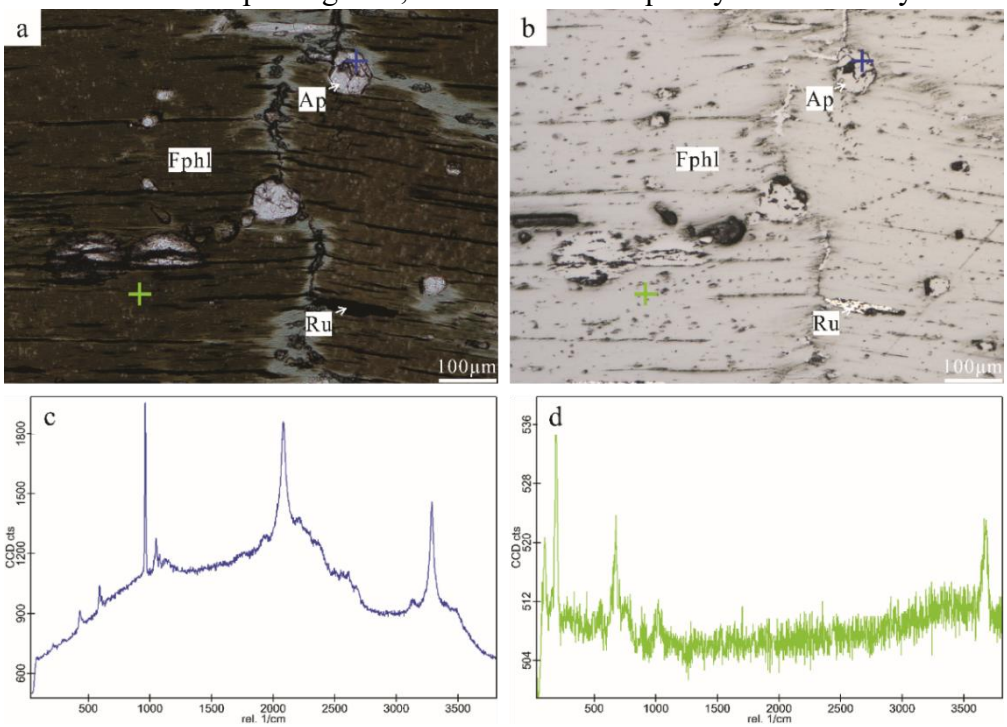

Fig. 3 Laser Raman spectra of the Heyu megaporphyritic coarse-grained monzogranite in the Baimiaogou molybdenum deposit. (a) Plane-polarized light image of biotite in the megaporphyritic coarse-grained monzogranite (Sample No. 0803-01); (b) Reflected light image of biotite in the megaporphyritic coarse-grained monzogranite (Sample No. 0803-01); (c) Laser Raman spectrum of apatite in the megaporphyritic coarse-grained monzogranite; (d) Laser Raman spectrum of biotite in the megaporphyritic coarse-grained monzogranite.

5. DISCUSSION

5.1. Mineral Evolution Sequence and Multi-stage Fluid Metasomatism

The textural and spectral characteristics of the mineral assemblages indicate that the primary rock-forming phases underwent intense, multi-stage fluid metasomatism. Plagioclase crystals are widely overprinted by patchy albite, reflecting interaction with sodium-rich fluids in an open system [17-19]. Raman spectroscopy confirms that the internal sericitized and argillized patches replace orthoclase, which itself formed via potassium metasomatism of earlier albite. Cross-cutting relationships and inclusion patterns define at least three distinct stages of silicification. Early-stage quartz hosts argillized plagioclase fragments, postdating the main albitization and K-feldspathization events. A subsequent generation of quartz includes hornblende and biotite, with the hornblende showing retrograde alteration to biotite, suggesting precipitation from a later silicon-rich fluid. A final silicification stage is represented by quartz that encloses perthite fragments with strongly dissolved margins. The perthite contains inclusions of residual plagioclase, quartz, and mafic phases, separated by irregular embayed boundaries or clean rims. These textures indicate that the perthite is not an early magmatic phase, but rather the product of early minerals intensely metasomatized by late potassium-rich alkaline fluids [20-25].

5.2. Micro-crystallographic Indications of Dark Minerals and Accessory

Minerals in Fine Veinlets Mafic phases (hornblende and biotite) are much finer-grained than the felsic framework. They fill intergranular fractures between plagioclase and quartz to form irregular veinlets, lacking the typical mosaic textures associated with magmatic co-crystallization. Hornblende and biotite frequently enclose albitized and K-feldspathized plagioclase remnants, showing that mafic mineral crystallization postdates the early alkaline metasomatism and silicification. Biotite cross-cuts hornblende along cleavage planes and fractures, and replaces hornblende margins to form pseudomorphs, reflecting an increasingly potassium-rich fluid composition over time. Accessory phases (apatite, sphene, zircon, and magnetite) are highly concentrated within these mafic veinlets, occurring as cross-cutting phases or aligning along cleavage planes, which indicates an even later precipitation timing. The localization of volatile-bearing (apatite) and high-field-strength element-enriched (sphene, zircon) minerals within micro-fractures reflects abrupt shifts in physical and chemical conditions, including temperature, pressure, and volatile solubility. Abundant euhedral magnetite indicates locally elevated oxygen fugacity. The spatial distribution and textural relationships of these veinlet assemblages confirm they precipitate from late, volatile-rich hydrothermal fluids filling micro-fractures rather than crystallizing via normal magmatic fractionation [26-28].

5.3. Reactivation Mechanism of Frozen Magma Chamber

The multi-stage hydrothermal metasomatism and the paragenetic sequence of the veinlet minerals provide direct microscopic evidence for the fluid evolution of the deep crystal mush. Based on petrographic observations, the crystallization and fluid evolution of the pluton proceed through three continuous stages.

The initial stage involves early crystallization and cold storage of the crystal mush. During the early fractional crystallization of the deep magmatic system, plagioclase precipitates to form a rigid crystal framework (65% to 70% by volume). The high crystallinity and low melt fraction result in a stagnant crystal mush within a relatively closed system[28-31]. These early-formed plagioclase crystals establish the primary structural framework of the intrusion.

The second stage is characterized by deep fluid injection and mush reactivation. Deep tectono-thermal events drive the large-scale influx of exogenous alkali-rich and volatile-rich supercritical fluids into

the mush. This injection generates internal pore fluid overpressure, fracturing the plagioclase framework and creating an interconnected network of micro-fractures. The system transitions from closed to open as high-temperature fluids penetrate the framework[18,28,32], resulting in pervasive patchy albitization of the early plagioclase megacrysts. As the fluid composition evolves, this sodium metasomatism is subsequently overprinted by intense potassium metasomatism. Such pervasive fluid-rock interaction sharply decreases the rheological viscosity of the crystal mush[33,34], allowing it to regain mobility and eruptive capacity [30].

The final stage includes magma emplacement and late-stage fluid precipitation. Lubricated by the invading fluids, the reactivated magma carrying the early plagioclase framework migrates to the shallow crust. Emplacement drives rapid decompression and cooling, causing significant fluctuations in the physicochemical state of the fluid. A decrease in fluid pH initiates the first stage of silicification [17]. Subsequent volatile supersaturation drives the crystallization of hydrous mafic minerals (hornblende and biotite) within the intergranular spaces. As high-field-strength elements and volatiles concentrate in the residual fluid, accessory minerals precipitate within the micro-fractures [35]. Continued cooling drives waning alkali metasomatism and multi-stage low-temperature silicification, finalizing the observed petrographic architecture.

6. CONCLUSION

The textural complexity and multi-stage hydrothermal overprints of the Heyu monzogranite record the complete evolutionary sequence of a high-silica magmatic system, spanning deep crystal mush storage, fluid reactivation, and final emplacement. The accumulated plagioclase framework records the initial closed-system cold storage stage, characterized by high crystallinity and minimal fluidity.

The influx of exogenous alkali- and volatile-rich supercritical fluids is the primary mechanism for overcoming the rheological barrier of the crystal mush. High-temperature fluid injection generates internal overpressures that fracture the plagioclase framework, facilitating intense albitization and subsequent K-feldspathization. This fluid-rock interaction sharply decreases the bulk viscosity of the mush, transitioning it to an open system and restoring its mobility.

Emplacement and final consolidation are controlled by continuous shifts in the physical and chemical state of the fluid. Rapid cooling and decompression trigger volatile supersaturation and acidity variations, driving the pervasive crystallization of hydrous mafic phases and high-field-strength element-enriched accessory minerals within intergranular fractures. The precipitation of these vein-hosted phases, combined with multiple stages of silicification, establishes the complex petrographic signature of the pluton.

REFERENCES

[1] Li Yongfeng. Spatiotemporal Evolution of Mesozoic Granitoids and Molybdenum (Gold) Mineralization in the Xiong'er Mountain Area, Western Henan. Beijing: China University of Geosciences (Beijing), 2005.

[2] Guo Bo. Geological and Geochemical Characteristics and Metallogenic Dynamic Background of the Jinduicheng Porphyry Molybdenum Deposit in East Qinling. Xi'an: Northwest University, 2009.

[3] Chen Yanjing, Zhai Mingguo, Jiang Shaoyong. Significant Advances and Issues in Orogenic Processes and Mineralization of the North China Continental Margin. Acta Petrologica Sinica, 2009, 25(11): 2695-2726.

[4] Ye H, Sun J, Wang S, et al. Geology and Genesis of the World-Class Donggou Porphyry Molybdenum Deposit, Henan Province, East Qinling Metallogenic Belt, Central China. Acta Geologica Sinica (English Edition), 2014, 88(s2): 635-636.

[5] Zhang Yanwei. Formation of Cryptoexplosive Breccia Pipe and Its Tectonic Dynamic Mechanism in the Mutougou Molybdenum Deposit, East Qinling. Shijiazhuang: Shijiazhuang University of Economics, 2015.

[6] Lu Xinxiang, Luo Zhaohua, Huang Fan, et al. Small Magma, Large Fluid, and Ore Formation Related to Transmagmatic Fluid: A Case Study of Molybdenum Deposits in the East Qinling–Dabie Orogenic Belt. Acta Petrologica Sinica, 2017, 33(5): 1554-1570.

[7] Li Congying, Liao Renqiang. Formation Mechanism and Geochemical Processes of Porphyry Molybdenum Deposits. Acta Petrologica Sinica, 2020, 36(1): 1-8.

[8] Qi N, Williams-Jones A E, Yu J, et al. The Geochronology, Geochemistry, and Petrogenesis of the Leimengou Porphyries, Qinling Orogen: A Case Study of Intrusions Associated with a Dabie-Type Porphyry Mo Deposit. Ore Geology Reviews, 2023, 163: 105781.

[9] Clemens J D, Petford N. Granitic Melt Viscosity and Silicic Magma Dynamics in Contrasting Tectonic Settings. Journal of the Geological Society, 1999, 156(6): 1057-1060.

[10] Wu Fuyuan, Liu Xiaochi, Ji Weiqiang, et al. Identification and Study of Highly Fractionated Granites. Scientia Sinica Terrae, 2017, 47(7): 745-765.

[11] Meng Q R, Zhang G W. Geologic Framework and Tectonic Evolution of the Qinling Orogen, Central China. Tectonophysics, 2000, 323(3): 183-196.

[12] Zhang Guowei. Qinling Orogenic Belt and Continental Dynamics. Beijing: Science Press, 2001.

[13] Zhang Guowei. Mianlue Tectonic Belt and Mianlue Suture Zone on the Southern Margin of the Qinling–Dabie Orogenic Belt. Science in China (Series D: Earth Sciences), 2003, 33(12): 1121-1135.

[14] Dong Yunpeng. Tectonic Attributes and Proterozoic Tectonic Evolution of the North Qinling. Acta Geoscientica Sinica, 2003, 24(1): 1-8.

[15] Zhang Guowei, Zhang Zongqing, Dong Yunpeng. Tectonic Nature of Major Tectono-Lithostratigraphic Units in the Qinling Orogenic Belt and Their Tectonic Significance. Acta Petrologica Sinica, 1995, 11(2): 101-114.

[16] Dong Y, Santosh M. Tectonic Architecture and Multiple Orogeny of the Qinling Orogenic Belt, Central China. Gondwana Research, 2016, 29(1): 1-40.

[17] Du Letian. Geochemical Principles of Alkali Metasomatism. Science in China (Series B: Chemistry, Biology, Agriculture, Medicine, Earth Sciences), 1986, 16(1): 81-90.

[18] Du Letian. Significant Genetic Implications of Alkali Metasomatites. Mineral Deposits, 2002, 21(S1): 953-958.

[19] Luo Zhaohua, Lu Xinxiang, Guo Shaofeng, et al. Transmagmatic Fluid Ore-Forming System. Acta Petrologica Sinica, 2008, 24(12): 2669-2678.

[20] Dong Shenbao, He Gaopin. Metasomatic Textures and Structures of Granitic Rocks and Their Genetic Significance. Bulletin of the Chinese Academy of Geological Sciences, 1987, (2): 71-82.

[21] Jin Wenshan. On the Genesis of Perthite and Antiperthite in Archean Migmatitic Complex Rocks. Collected Works of Tianjin Institute of Geology and Mineral Resources, Chinese Academy of Geological Sciences (No. 19). Beijing: Geological Publishing House, 1988: 112-123.

[22] Putnis A. Mineral Replacement Reactions: From Macroscopic Observations to Microscopic Mechanisms. Mineralogical Magazine, 2002, 66(5): 689-708.

[23] Omella M E, Gong Enpu, Sun Xudong, et al. Perthite Formed by Potassium Replacement of Plagioclase in Granites from Zhejiang Province. Geology and Resources, 2003, 12(3): 129-138.

[24] Parsons I, Fitz Gerald J D, Heizler M T, et al. Eight-Phase Alkali Feldspars: Low-Temperature Cryptoperthite, Peristerite and Multiple Replacement Reactions in the Klokken Intrusion. Contributions to Mineralogy and Petrology, 2013, 165(5): 931-960.

[25] Liu Lulu. Characteristics, Genesis and Metallogenic Significance of Tanling Plagioclase Porphyry in Wu'an, Hebei Province. Beijing: China University of Geosciences (Beijing), 2017.

[26] Su Shangguo, Cui Xiaoliang, Luo Zhaohua, et al. Fluid Crystals, Fluid Crystal Mineral Assemblages, Fluid Rocks and Their Research Significance. Earth Science Frontiers, 2018, 25(6): 283-289.

[27] Liu Lulu, Su Shangguo, Yang Ruina, et al. Characteristics of Matrix Minerals in the Tanling Multiple Plagioclase Porphyry in Wu'an, Hebei Province and Their Significance. Earth Science Frontiers, 2019, 26(1): 286-299.

[28] Luo Zhaohua, Yang Zongfeng, Su Shangguo, et al. Supercritical Fluid Crystals in Igneous Rocks and Their Research Significance. Earth Science Frontiers, 2019, 26(6): 216-227.

[29] Liu Lulu, Su Shangguo, Hou Jianguang, et al. Genesis of Tanling Multiple Plagioclase Porphyry in Wu'an, Hebei Province: Reactivation Mechanism of Frozen Magma Chamber. Acta Petrologica Sinica, 2017, 33(1): 204-220.

[30] Ma Changqian, Zou Bowen, Gao Ke, et al. Crystal Mush Storage, Intrusive Accumulation and Granite Genesis. Earth Science, 2020, 45(12): 4332-4351.

[31] Humphreys M C S, Namur O, Bohrson W A, et al. Crystal Mush Processes and Crustal Magmatism. Nature Reviews Earth & Environment, 2025, 6(6): 401-416.

[32] Xu Xingwang. Fluid Tectodynamics and Its Research Status and Progress. Advances in Earth Science, 2001, 16(3): 324-331.

[33] Huber C, Bachmann O, Dufek J. Thermo-Mechanical Reactivation of Locked Crystal Mushes: Melting-Induced Internal Fracturing and Assimilation Processes in Magmas. Earth and Planetary Science Letters, 2011, 304(3): 443-454.

[34] Parmigiani A, Huber C, Bachmann O. Mush Microphysics and the Reactivation of Crystal-Rich Magma Reservoirs. Journal of Geophysical Research: Solid Earth, 2014, 119(8): 6308-6322.

[35] Bacon C R. Crystallization of Accessory Phases in Magmas by Local Saturation Adjacent to Phenocrysts. Geochimica et Cosmochimica Acta, 1989, 53(5): 1055-1066.